

cesses.

¹⁶One can obtain an indication of the temperature dependency of the parameters through decay studies at constant T . Decay, for constant parameters, yields no information which is not already contained in the TSL and TSC curves; if the parameters are temperature dependent, however, then the decay pattern will be inconsistent with the pre-

sumed (constant) parametric description of the curves, and thus will provide a warning that the assumed model is too simple.

¹⁷M. Schön, *Tech. Wiss. Abhandl. Osram-Ges.* **7**, 175 (1958).

¹⁸P. Bräunlich, *J. Appl. Phys.* **39**, 2953 (1967).

Electron Paramagnetic Resonance of the Neutral ($S=1$) One-Vacancy-Oxygen Center in Irradiated Silicon[†]

K. L. Brower

Sandia Laboratories, Albuquerque, New Mexico 87115

(Received 10 August 1970)

A new EPR spectrum, labeled Si-S1, has been observed in electron- or neutron-irradiated, n - or p -type, crucible-grown silicon under illumination with approximately band-gap light. The Si-S1 spectrum consists primarily of a fine-structure spectrum and a ²⁹Si hyperfine spectrum. By incorporating ¹⁷O atoms into vacuum-float-zone silicon by ion implantation, the Si-S1 ¹⁷O hyperfine spectrum was also observed. An analysis of the coupling tensors in the spin Hamiltonian which characterize the fine structure and ²⁹Si hyperfine spectrum is presented and suggests that the Si-S1 center is the neutral charge state of the one-vacancy-oxygen center in an excited spin-triplet state. This model for the Si-S1 center is in agreement with stress measurements, which are also presented. These measurements indicate that the time-temperature dependence in the reorientation of the Si-S1 center is the same as that of the neutral one-vacancy-oxygen center as monitored by the Si-B1 spectrum.

I. INTRODUCTION

Previous studies have shown that the dominant paramagnetic centers that are formed in electron-irradiated, crucible-grown silicon at room temperature are the Si-B1 center¹⁻⁴ and the Si-G15 (oxygen-associated) center.⁵⁻⁶ The Si-B1 center was previously identified¹⁻⁴ as the negative charge state of the one-vacancy-oxygen center. Recently it has been shown that these centers also exist in low-fluence fast-neutron-irradiated crucible-grown silicon.⁷ In looking at irradiated silicon samples under illumination with electron paramagnetic resonance (EPR), we have found a new spin-1 spectrum, labeled Si-S1, which is prevalent in n - and p -type, electron- or neutron-irradiated, crucible-grown silicon. The Si-S1 spectrum is also observed in some samples of LOPEX and vacuum-float-zone silicon, but the intensity of the spectrum is less than that observed in crucible-grown silicon by at least a factor of 20. In this paper we report many of the outstanding features that are observed in the Si-S1 spectrum. A detailed analysis of the Si-S1 spectrum is presented and indicates that the Si-S1 center is the neutral one-vacancy-oxygen center in an excited spin-triplet state.

The electronic and molecular structure of the Si-S1 center is deduced from an unusually rich

EPR spectrum. Section II discusses briefly the experimental aspects of the EPR measurements. The analysis of the Si-S1 spectrum in Sec. III deals with the development of the appropriate spin Hamiltonian, the constraints on the coupling tensors in this spin Hamiltonian, and the numerical analysis and values for the coupling tensors as deduced from the Si-S1 spectrum. An analysis of the coupling tensors in terms of the physical interactions which they represent is presented in Sec. IV and shows how the structure of the Si-S1 center evolves from this analysis. We have also succeeded in correlating the Si-S1 center with the Si-B1 center through the time-temperature dependence in the reorientation of these centers.

II. EXPERIMENT

The samples used in the study of the Si-S1 center were crucible-grown n -type silicon (P-doped, 0.04–10 Ω cm) and p -type silicon (B-, Al-, or Ga-doped, 0.7–5 Ω cm). These samples were irradiated at room temperature with 2-MeV electrons with fluences up to 3×10^{17} e/cm². The spectrum of the Si-S1 center which is seen in n - or p -type, electron-irradiated, crucible-grown silicon for $\vec{H} \parallel [110]$ is shown in Fig. 1. The Si-S1 center is also observed in neutron-irradiated crucible-grown silicon for fluences $\lesssim 10^{17}$ n/cm². The Si-S1 spectrum was also observed in some samples of

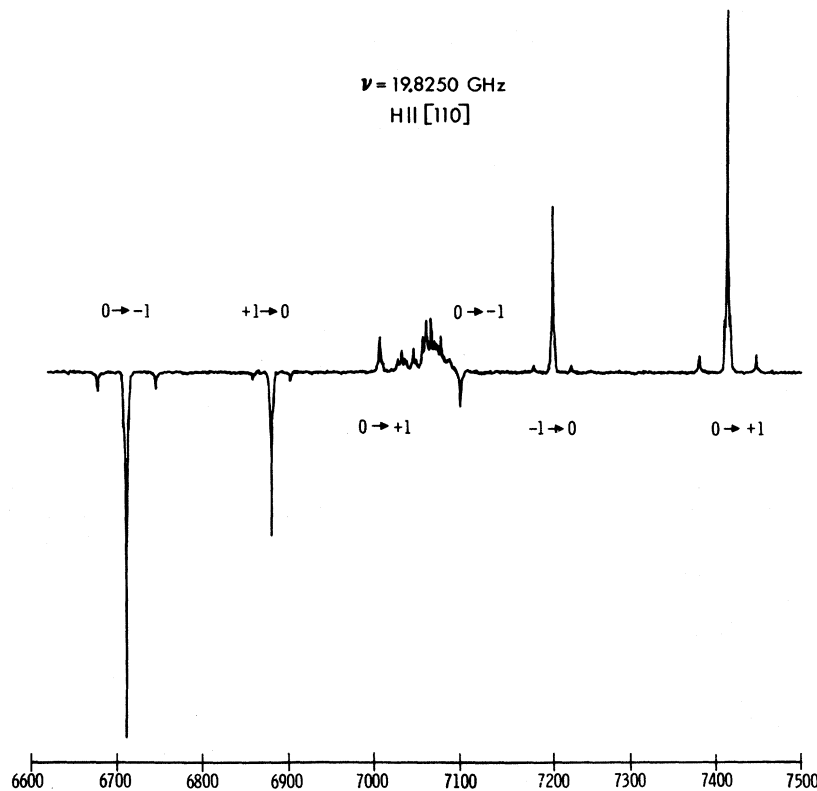


FIG. 1. EPR spectrum observed under illumination in Al-doped crucible-grown silicon following a 2-MeV electron irradiation of $5 \times 10^{16} e/cm^2$. The lines at 6710, 6880, 7010, 7100, 7200, and 7410 Oe constitute the Si-S1 center for $\vec{H} \parallel [110]$. Part of the spectrum at ~ 7060 Oe corresponds to the Si-G15 center. The identification of the states $|S=1, M\rangle$, which are defined within the strong field approximation, between which the transitions occur is discussed in Sec. III B.

LOPEX and vacuum-float-zone silicon, but its intensity was less than that observed in crucible-grown silicon by at least a factor of 20. In order to verify the existence of oxygen in the Si-S1 center, a sample of intrinsic vacuum-float-zone silicon was implanted with 200-keV $^{17}\text{O}^+$ ions to a fluence of $3 \times 10^{14} \text{ O}^+/cm^2$. (^{17}O has a nuclear spin of $\frac{5}{2}$.) This sample was annealed at 300, 600, and 960 °C for 20 min and then annealed at 400 °C for 10 min. In order to produce Si-S1 centers, the implanted region was then damaged by 280-keV $^4\text{He}^+$ ions to a fluence of $10^{13} \text{ He}^+/cm^2$. The existence of the Si-S1 center does not appear to depend upon the presence of either group-III or -V impurities. The Si-S1 center was not observed in unirradiated silicon.

Between 5 and ~ 100 K, we were only able to observe the Si-S1 spectrum with the sample illuminated. Between ~ 100 and ~ 300 K, we were unable to observe the Si-S1 spectrum with or without illumination. The samples were illuminated in our K-band TE_{011} cylindrical copper cavity by a sub-miniature lamp mounted in the wall of the cavity. The intensity of the Si-S1 spectrum was observed to be proportional to the voltage across the sub-miniature lamp for voltages up to burnout. Our X-band TE_{103} rectangular cavity incorporated an optical window which consisted of a mesh of 0.050-in.-diam holes in one wall opposite the sample through which light entered from the outside. (The

cryostat has a sapphire window opposite the cavity window.) By means of various infrared filters, optical filters, and slices of polished silicon and GaAs, we conclude that the Si-S1 spectrum is generated by approximately band-gap light. To see whether we were generating paramagnetic Si-S1 centers near the illuminated surface or throughout the bulk of the sample, the volume of the X-band sample was reduced by $\frac{3}{4}$ while keeping the illuminated surface area constant. The intensity of the signal was found to be approximately proportional to the sample volume.

The EPR measurements were made with an X-band (9.5 GHz) and a K-band (19.9-GHz) superheterodyne spectrometer. The spectra were taken in the dispersion mode. The magnetic field at the sample had previously been calibrated to $\lesssim 0.3$ Oe in terms of the magnetic field at the position of the NMR probe on the outside of the Dewar which had a brass tail. Small adjustments in the orientation of the table supporting the cryostat and spectrometers allowed us to align the crystallographic directions of the sample to within 0.1° of the direction of the magnetic field.

III. ANALYSIS OF THE Si-S1 SPECTRUM

A. Spin Hamiltonian

The spin Hamiltonian for a pair of interacting electrons localized on a defect within a crystal can be written in the form

$$\mathcal{H} = \frac{1}{2} \begin{bmatrix} \vec{H} \\ \vec{S}_1 \\ \vec{S}_2 \\ \vec{I}_1 \\ \cdot \\ \cdot \\ \cdot \\ \vec{I}_m \end{bmatrix}^\dagger \begin{bmatrix} 2\vec{C} & \mu_B \vec{g}_1 & \mu_B \vec{g}_2 & \mu_n \vec{\gamma}_1 & \dots & \mu_n \vec{\gamma}_m \\ \mu_B \vec{g}_1^\dagger & 0 & \vec{K} & \vec{A}_{11} & \dots & \vec{A}_{1m} \\ \mu_B \vec{g}_2^\dagger & \vec{K}^\dagger & 0 & \vec{A}_{21} & \dots & \vec{A}_{2m} \\ \mu_n \vec{\gamma}_1^\dagger & \vec{A}_{11}^\dagger & \vec{A}_{21}^\dagger & 2\vec{Q}_{11} & \dots & \vec{Q}_{1m} \\ \cdot & \cdot & \cdot & \cdot & \cdot & \cdot \\ \cdot & \cdot & \cdot & \cdot & \cdot & \cdot \\ \cdot & \cdot & \cdot & \cdot & \cdot & \cdot \\ \mu_n \vec{\gamma}_m^\dagger & \vec{A}_{1m}^\dagger & \vec{A}_{2m}^\dagger & \vec{Q}_{1m}^\dagger & \dots & 2\vec{Q}_{mm} \end{bmatrix} \begin{bmatrix} \vec{H} \\ \vec{S}_1 \\ \vec{S}_2 \\ \vec{I}_1 \\ \cdot \\ \cdot \\ \cdot \\ \vec{I}_m \end{bmatrix} \quad (1)$$

This spin Hamiltonian is quadratic and bilinear in \vec{H} , \vec{S}_i , and \vec{I}_j , where \vec{H} is the magnetic field, S_i are the electron-spin operators, and I_j are the nuclear-spin operators. The various interactions between \vec{H} , \vec{S}_i , and \vec{I}_j are specified in terms of the coupling tensors. The \vec{C} tensor accounts for terms quadratic in the magnetic field.⁸ EPR spectra are insensitive to this interaction because it shifts all of the eigenvalues of \mathcal{H} for a given magnetic field by the same amount. This interaction is generally ignored by setting the \vec{C} tensor equal to zero. The electronic Zeeman interaction is specified by the g_1 and g_2 tensors contained within the terms $\mu_B \vec{H} \cdot g_1 \cdot \vec{S}_1 + \mu_B \vec{H} \cdot g_2 \cdot \vec{S}_2$ of Eq. (1). The interaction between the two paramagnetic electrons, commonly referred to as the electronic spin-spin interaction, is specified by the \vec{K} tensor and corresponds to the term $\vec{S}_1 \cdot \vec{K} \cdot \vec{S}_2$ of Eq. (1). It is usually convenient to write the \vec{K} tensor as the sum of an isotropic term J , where $J = \text{Tr} \frac{1}{3}(\vec{K})$, a symmetric term \vec{D} , where $\text{Tr}(\vec{D}) = 0$, and an antisymmetric term \vec{a} . If there are nuclei with nonzero magnetic moments in the neighborhood of the paramagnetic center, then these nuclei may interact with the paramagnetic electrons giving resolved hyperfine spectra. The hyperfine interactions are specified

by the \vec{A}_{ij} tensors and correspond to terms of the form $\vec{S}_i \cdot \vec{A}_{ij} \cdot \vec{I}_j$ in Eq. (1). The nuclear quadrupole interaction $\vec{I}_j \cdot \vec{Q}_{ij} \cdot \vec{I}_j$ is characterized by the \vec{Q}_{ij} tensor for nuclei with $I_j > \frac{1}{2}$. The \vec{Q}_{ij} tensor is necessarily equal to zero for nuclei with I_j equal to $\frac{1}{2}$. The nuclear spin-spin interaction arises from terms of the form $\vec{I}_k \cdot \vec{Q}_{ki} \cdot \vec{I}_i$ ($k \neq i$) in Eq. (1).

A set of basis spin states for determining the eigenvalues and eigenvectors of this spin Hamiltonian consists of states of the form $|S_1, S_{1z}; S_2, S_{2z}; I_1, m_1; \dots; I_m, m_m\rangle$ where S_1 and S_2 equal $\frac{1}{2}$. In the case of the Si-S1 center, the impurity dependence of this defect (see Sec. II) indicates that the nuclear-spin interactions are expected to arise from the ^{29}Si ($I = \frac{1}{2}$, 4.70% naturally abundant) and possibly the ^{17}O ($I = \frac{5}{2}$, 0.037% naturally abundant) isotopes.

B. Constraints on Coupling Tensors

Kneubühl,^{9,10} Bieri *et al.*,¹¹ and Baltes *et al.*¹² have shown how the most general forms for the coupling tensors compatible with the symmetry of a polyatomic paramagnetic center can be determined for a spin Hamiltonian of the form in Eq. (1). Using this group theoretical approach, we have determined the constraints on the coupling tensors for two

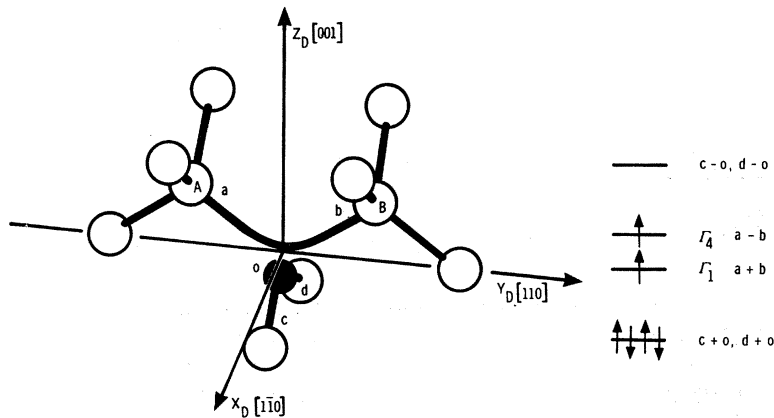


FIG. 2. Electronic structure of the one-vacancy-oxygen center having C_{2v} symmetry in an excited spin-triplet state. The linear combination of orbitals which transform according to the various irreducible representations of the point group C_{2v} are indicated.

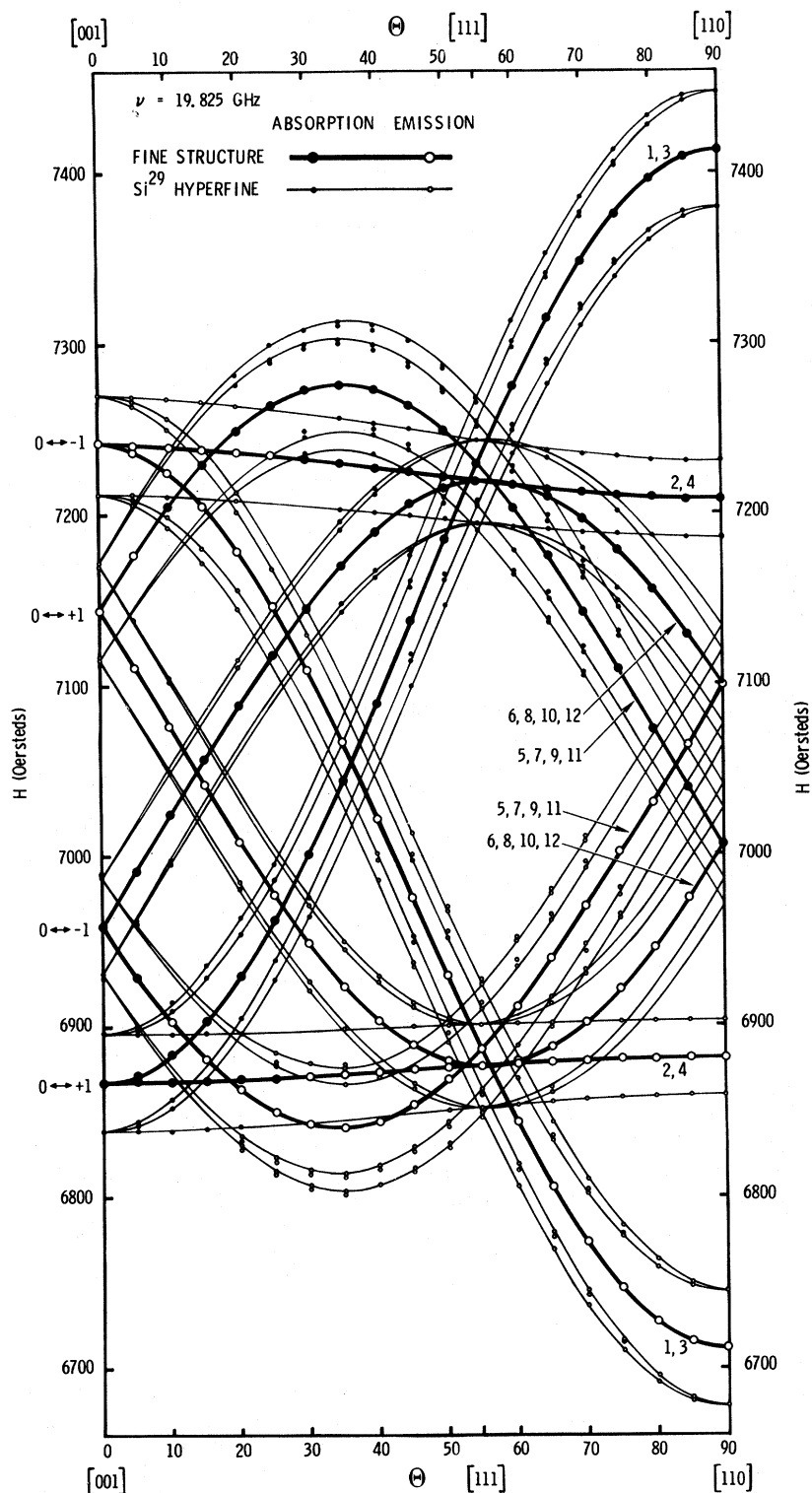


FIG. 3. Map of the Si-S1 EPR spectrum as observed at *K* band. The solid lines correspond to the calculated Si-S1 spectrum using the coupling tensors in Table II. The circles and dots correspond to the observed resonances. The transitions for the fine-structure spectrum have been labeled in terms of the states $|S=1, M\rangle$ defined in the strong field approximation.

isotopic configurations of the one-vacancy-oxygen center. (Evidence for the assignment of this model to the Si-S1 center will be presented in Sec. IV.) The $^{28}\text{Si}-^{16}\text{O}-^{28}\text{Si}$ configuration consists of ^{16}O at site *O* and ^{28}Si isotopes at *A* and *B* in Fig. 2. This

configuration has C_{2v} symmetry and gives rise to the fine-structure spectrum in Fig. 3. The $^{29}\text{Si}-^{16}\text{O}-^{28}\text{Si}$ configuration consists of an ^{16}O at site *O*, a ^{29}Si at site *A* and a ^{28}Si at site *B*, or vice versa. This configuration has C_s symmetry and accounts

TABLE I. Tabulation of the general and reduced forms of the coupling tensors belonging to the spin Hamiltonian in Eq. (1). The principal axes are defined in Fig. 2 with respect to the defect. The general form as well as the reduced form of these coupling tensors give spectra whose degeneracies for H along the [001], [111], and [110] correspond to the observed degeneracies in Fig. 3.

Ten- sors	Fine-structure spectrum $^{28}\text{Si}-^{16}\text{O}-^{28}\text{Si}$ configuration		^{29}Si hyperfine spectrum $^{29}\text{Si}-^{16}\text{O}-^{28}\text{Si}$ configuration	
	General form of coupling tensors (Ref. 12)	Reduced form of coupling tensors	General form of coupling tensors	Reduced form of coupling tensors
g_1	$\begin{pmatrix} g_{xx} & 0 & 0 \\ 0 & g_{yy} & g_{yz} \\ 0 & g_{zy} & g_{zz} \end{pmatrix}$	$\begin{pmatrix} g_{xx} & 0 & 0 \\ 0 & g_{yy} & 0 \\ 0 & 0 & g_{zz} \end{pmatrix}$	$\begin{pmatrix} g_{xx} & 0 & 0 \\ 0 & g_{yy} & g_{yz} \\ 0 & g_{zy} & g_{zz} \end{pmatrix}$	$\begin{pmatrix} g_{xx} & 0 & 0 \\ 0 & g_{yy} & 0 \\ 0 & 0 & g_{zz} \end{pmatrix}$
g_2	$\begin{pmatrix} g_{xx} & 0 & 0 \\ 0 & g_{yy} & -g_{yz} \\ 0 & -g_{zy} & g_{zz} \end{pmatrix}$	$\begin{pmatrix} g_{xx} & 0 & 0 \\ 0 & g_{yy} & 0 \\ 0 & 0 & g_{zz} \end{pmatrix}$	$\begin{pmatrix} g'_{xx} & 0 & 0 \\ 0 & g'_{yy} & g'_{yz} \\ 0 & g'_{zy} & g'_{zz} \end{pmatrix}$	$\begin{pmatrix} g_{xx} & 0 & 0 \\ 0 & g_{yy} & 0 \\ 0 & 0 & g_{zz} \end{pmatrix}$
K	$\begin{pmatrix} K_{xx} & 0 & 0 \\ 0 & K_{yy} & K_{yz} \\ 0 & -K_{yz} & K_{zz} \end{pmatrix}$	$\begin{pmatrix} K_{xx} & 0 & 0 \\ 0 & K_{yy} & 0 \\ 0 & 0 & K_{zz} \end{pmatrix}$	$\begin{pmatrix} K_{xx} & 0 & 0 \\ 0 & K_{yy} & K_{yz} \\ 0 & K_{zy} & K_{zz} \end{pmatrix}$	$\begin{pmatrix} K_{xx} & 0 & 0 \\ 0 & K_{yy} & 0 \\ 0 & 0 & K_{zz} \end{pmatrix}$
γ_1	$\begin{pmatrix} \gamma_{xx} & 0 & 0 \\ 0 & \gamma_{yy} & \gamma_{yz} \\ 0 & \gamma_{zy} & \gamma_{zz} \end{pmatrix}$	$\begin{pmatrix} \gamma & 0 & 0 \\ 0 & \gamma & 0 \\ 0 & 0 & \gamma \end{pmatrix}$
A_{11}	$\begin{pmatrix} A_{xx} & 0 & 0 \\ 0 & A_{yy} & A_{yz} \\ & A_{zy} & A_{zz} \end{pmatrix}$	$\begin{pmatrix} A_{xx} & 0 & 0 \\ 0 & A_{yy} & A_{yz} \\ 0 & A_{zy} & A_{zz} \end{pmatrix}$
A_{21}	$\begin{pmatrix} A'_{xx} & 0 & 0 \\ 0 & A'_{yy} & A'_{yz} \\ 0 & A'_{zy} & A'_{zz} \end{pmatrix}$	$\begin{pmatrix} A_{xx} & 0 & 0 \\ 0 & A_{yy} & A_{yz} \\ 0 & A_{zy} & A_{zz} \end{pmatrix}$

for the ^{29}Si hyperfine spectrum in Fig. 3. The relative intensity of the fine-structure spectrum to the ^{29}Si hyperfine spectrum is observed to be $\sim 10:1$. More complex isotopic configurations involving additional sites are either relatively improbable or do not give well-resolved spectra. The minimal constraints on the coupling tensors for these two isotopic configurations are tabulated in Table I.

It is interesting to note that these coupling tensors are asymmetric. Furthermore, nonzero matrix elements of \mathcal{H} can exist between the triplet and singlet states. The results of our analysis (see Sec. III C) indicate that in the case of the Si-S1 center, the perturbation in the triplet levels due to the interaction with the singlet level is small compared to the perturbation in the triplet levels due to the nuclear Zeeman interaction. The reduced

coupling tensors for an approximate spin Hamiltonian, which involves no coupling between the triplet and singlet manifolds, are tabulated in Table I. This spin Hamiltonian also describes the Si-S1 spectrum quite accurately (see Sec. III C) and is adequate for describing many of the features in the spectrum.

The Si-S1 spectrum has at least two characteristics which place restrictions on the signs of the coupling tensors. The first characteristic in the observed spectrum is the positive and negative intensities of the resonances illustrated in Figs. 1 and 4. As a result of populating the spin-triplet levels of the Si-S1 center by light, a population inversion is achieved within the spin-triplet levels. This population inversion is manifested by spin-resonance lines of negative intensity (stimulated emission transitions) and positive intensity (stimulated

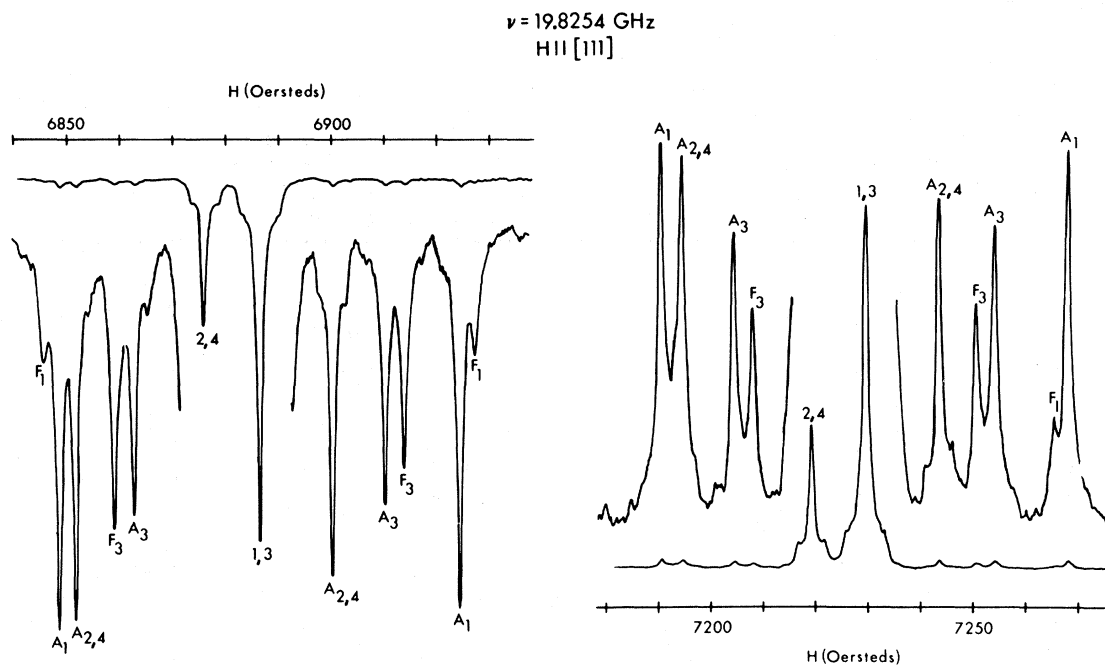


FIG. 4. EPR spectrum of the Si-S1 center for $\vec{H} \parallel [111]$ observed in Al-doped crucible-grown silicon following a 2-MeV electron irradiation of $5 \times 10^{16} e/cm^2$. The allowed transitions are labeled A_n and the forbidden transitions F_n . The subscript denotes at least one of the degenerate coordinate frames. The relative transition probability as calculated from the eigenvectors of Eq. (1) using the coupling tensors in Table II for each of the ^{29}Si hyperfine lines in coordinate frame 1 or 3 is (from left to right): $F_1 \sim 0.09$, $A_1 \sim 0.41$, $F_3 \sim 0.24$, $A_3 \sim 0.26$, $A_3 \sim 0.26$, $F_3 \sim 0.23$, $A_1 \sim 0.41$, $F_1 \sim 0.09$; $A_1 \sim 0.43$, $A_3 \sim 0.29$, $F_3 \sim 0.21$, $F_3 \sim 0.21$, $A_3 \sim 0.29$, $F_1 \sim 0.07$, and $A_1 \sim 0.43$. These results agree reasonably well with the observed intensities.

absorption transitions).¹³ The relative intensity of the lines in the Si-S1 spectrum is observed to be a function of the magnetic field orientation. These effects are like those observed in excited spin-triplet levels by Tanimoto, Ziniker, and Kemp,¹⁴ and Watkins.¹⁵ In Fig. 1, the intensity of the line at ~ 6710 Oe is approximately twice the intensity of the line at ~ 6880 Oe. However, according to the map of the Si-S1 spectrum in Fig. 3, the line at ~ 6710 Oe arises from defects in coordinate frames 1 and 3 while the line at ~ 6880 Oe arises from defects in coordinate frames 2 and 4.¹⁶ Under conditions of thermal equilibrium, these two lines would have equal intensities.

These experimental results indicate that for $\vec{H} \parallel [110]$ and for defects in coordinate frames 1 and 3, only the spin-triplet level $|1, 0\rangle$ is populated with electrons by light. Consequently, the resonance at ~ 6710 Oe corresponds to the $|1, 0\rangle$ to $|1, -1\rangle$ emissive transition. For those defects in coordinate frames 2 and 4, the two Zeeman levels corresponding to the $|1, \pm 1\rangle$ states are equally populated with electrons by light excitation. Consequently, the resonance at ~ 6880 Oe corresponds to the $|1, 1\rangle$ to $|1, 0\rangle$ emissive transition. Since only about half of the electrons are in the $|1, 1\rangle$ state for defects in coordinate frames 2 and

4, the line at 6880 Oe is only about half as intense as the line at ~ 6710 Oe.

It is on the basis of these arguments that the states between which transitions occur have been assigned to the resonances in Figs. 1 and 3. Knowing the states between which transitions occur allows us to impose the first set of restrictions on the signs of the \vec{g} , \vec{D} (symmetric part of \vec{K}), and \vec{A} reduced coupling tensors. In Fig. 5, the hypothetical spectra as deduced from the exact eigenvalues of Eq. (1) using the reduced coupling tensors are tabulated for all possible permutations in the signs of the \vec{g} , \vec{D} , and \vec{A} tensors. These calculations were carried out for the case in which $\vec{H} \parallel [111]$, and the defect is in coordinate frame 1. In Fig. 5 we have indicated whether the polarity of the hypothetical spectrum for each set of signs agrees or disagrees with the polarity of the observed spectrum in Fig. 4. As long as the differences between the reduced coupling tensors and the general coupling tensors are small so that the added perturbation in the energy levels is small compared to that arising from the nuclear Zeeman interaction, the signs of these remaining elements remain unrestricted. This condition holds for the Si-S1 coupling tensors.

The second characteristic of the Si-S1 spectrum

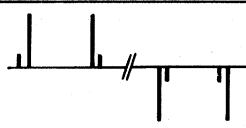
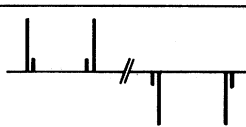
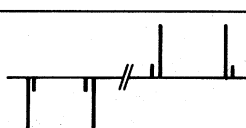
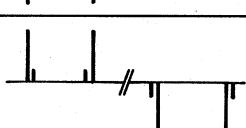
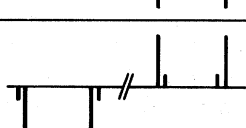
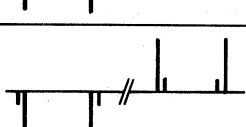
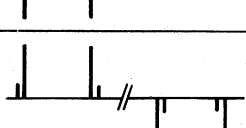
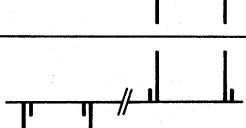
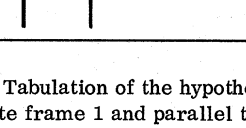
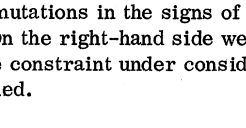
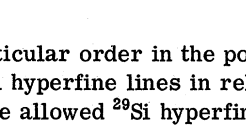
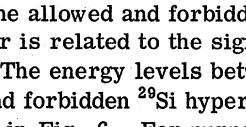
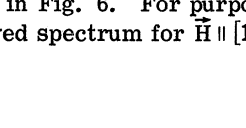

SIGN \vec{g} TENSOR	SIGN OF D_{yy}	SIGN \vec{A} TENSOR	LOW FIELD ^{29}Si HYPERFINE SPECTRUM $H \parallel [111]$	HIGH FIELD ^{29}Si HYPERFINE SPECTRUM	SIGNAL POLARITY FOR EMISSION AND ABSORPTION LINES	ORDER OF ALLOWED AND FORBIDDEN ^{29}Si HYPERFINE LINES	SIGN OF \vec{g} TENSOR RELATIVE TO SIGN OF \vec{A} TENSOR
+	+	+			X	OK	X
+	+	-			X	X	OK
+	-	+			OK	X	X
-	+	+			X	X	OK
+	-	-			OK	OK	OK
-	-	+			OK	OK	OK
-	+	-			X	OK	X
-	-	-			OK	X	X

FIG. 5. Tabulation of the hypothetical spectra for \vec{H} in coordinate frame 1 and parallel to the $[111]$ direction for all permutations in the signs of the \vec{g} , \vec{D} , and \vec{A} tensors. On the right-hand side we have indicated whether the constraint under consideration is satisfied or unsatisfied.

is the particular order in the positions of the forbidden ^{29}Si hyperfine lines in relation to the positions of the allowed ^{29}Si hyperfine lines. The order in which the allowed and forbidden ^{29}Si hyperfine lines occur is related to the signs of the coupling tensors. The energy levels between which the allowed and forbidden ^{29}Si hyperfine lines originate are shown in Fig. 6. For purposes of comparison, the observed spectrum for $\vec{H} \parallel [111]$ is shown in

Fig. 4 where the resonances labeled A_1 and F_1 correspond to the allowed and forbidden ^{29}Si hyperfine lines, respectively, arising from defects in coordinate frames 1, 5, and 9. In Fig. 5, we have indicated whether the order of the observed forbidden and allowed ^{29}Si hyperfine lines agrees or disagrees with that of the hypothetical spectra.

In addition to these restrictions, the expression for the Fermi-contact hyperfine interaction

$$a = \frac{8}{3} \pi g \mu_N (\mu_n/I) \mu_B |\psi(0)|^2 \quad (2)$$

indicates that there is a relationship between the sign of the \vec{g} tensor and the \vec{A} tensor [$a = \text{Tr} \frac{1}{3}(\vec{A})$]. Since $\mu_n = -0.55477 \mu_N$ for ^{29}Si ,¹⁷ the sign of the \vec{g} tensor is expected to be opposite the sign of the \vec{A} tensor. In Fig. 5, we have indicated whether the sign of the \vec{g} tensor relative to the sign of the \vec{A} tensor is consistent or inconsistent with the Fermi-contact hyperfine interaction.

The results of this analysis indicate that of the eight possible sign configurations for the \vec{g} , \vec{D} , and \vec{A} reduced coupling tensors, only two sign configurations are compatible with all three constraints simultaneously. One sign configuration is for $+\vec{g}$, $+D_{xx}$, $-D_{yy}$, $+D_{zz}$, and $-\vec{A}$; and the other sign configuration is for $-\vec{g}$, $+D_{xx}$, $-D_{yy}$, $+D_{zz}$, and $+\vec{A}$. The sign of the reduced \vec{D} tensor is the same for these two cases and has been determined unambiguously.

C. Numerical Analysis and Results

1. $^{28}\text{Si}-^{16}\text{O}-^{28}\text{Si}$ Configuration

For the case of the $^{28}\text{Si}-^{16}\text{O}-^{28}\text{Si}$ configuration, closed analytical expressions for the exact eigenvalues were obtained within the singlet-triplet manifold by diagonalizing the spin Hamiltonian in Eq. (1) subject to the constraints in Table I. The numerical values for the \vec{g} and \vec{K} tensors were determined by minimizing

$$\sum_i [\nu_{i, \text{expt}} - \nu_{i, \text{calc}}(H_{i, \text{expt}}, \theta_i, \vec{g}, \vec{K})]^2$$

by a method of least squares¹⁸ as a function of \vec{g}

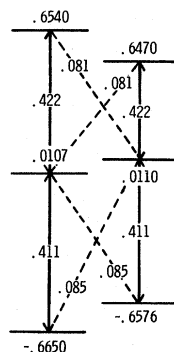


FIG. 6. Energy-level diagram within the triplet manifold for the $^{28}\text{Si}-^{16}\text{O}-^{28}\text{Si}$ configuration. The relative eigenvalues and transition probabilities were calculated for $\vec{H} \parallel [111]$ in Fig. 2 for $H=7000$ Oe. The vertical solid lines correspond to the allowed magnetic dipole transitions whereas the dotted lines correspond to the forbidden ^{29}Si hyperfine transitions.

TABLE II. Tabulation of the numerical values for the elements in the coupling tensors of Eq. (1). The principal axes for these elements are defined with respect to the defect in Fig. 2. The coupling tensors associated with the $^{28}\text{Si}-^{16}\text{O}-^{28}\text{Si}$ configuration were fitted to the X- and K-band fine-structure spectra with a standard deviation of $\sim 5.4 \times 10^{-4}$ GHz (~ 0.2 Oe) for values of J ranging from 5 to 100 cm^{-1} . The coupling tensors associated with the $^{29}\text{Si}-^{16}\text{O}-^{28}\text{Si}$ configuration subject to the additional constraints discussed in Sec. III C 2 were fitted to the X- and K-band ^{29}Si hyperfine spectra with a standard deviation of $\sim 2.9 \times 10^{-5}$ cm^{-1} (~ 0.3 Oe) for J arbitrarily equal to 50 cm^{-1} .

g tensor ± 0.0001					D tensor (in units of 10^{-4}cm^{-1}) ± 0.1				A tensor (in units of 10^{-4}cm^{-1}) ± 0.3				
g_{xx}	g_{yy}	g_{zz}	g_{yz}^2/J (cm^{-1})	g_{zy}^2/J (cm^{-1})	D_{xx}	D_{yy}	D_{zz}	D_{yz}^2/J	A_{xx}	A_{yy}	A_{zz}	A_{yz}	A_{zy}
2.0102 ₀	2.0057 ₆	2.0075 ₇	$\lesssim 2 \times 10^{-4}$	$\lesssim 3 \times 10^{-5}$	204.8 ₀	-438.3 ₁	233.5 ₁	$\lesssim 1 \times 10^{-4}$	-41.1 ₅	-61.3 ₂	-51.2 ₆	-15.5 ₂	-14.3 ₁

and \bar{K} for fixed J (eight parameters). The ν is the resonant microwave frequency. This analysis was carried out on 28 fine structure resonances from the X- and K-band Si-S1 spectra for \bar{H} along the [001], [111], and [110] directions.

The final numerical results for the coupling tensors belonging to the $^{28}\text{Si}-^{16}\text{O}-^{28}\text{Si}$ configuration are tabulated in Table II. This analysis indicates that the \bar{K} tensor is symmetric within the accuracy of our measurements. Furthermore, our analysis indicates that the coupling between the singlet and triplet states is negligible. If K_{23} , g_{23} , and g_{32} are assumed to be zero (the \bar{g} and \bar{K} tensors then correspond to the reduced \bar{g} and \bar{K} tensors in Table I) so that there is no coupling between the singlet and triplet states, then the calculated magnetic field positions of the resonances are shifted by ~ 0.1 Oe. This is less than the standard deviation of our least-squares fit which is ~ 0.2 Oe. Consequently, the numerical values for K_{23}^2/J , g_{23}^2/J , and g_{32}^2/J in Table II correspond to the approximate upper limits on these ratios.

We have been unable to observe the Si-S1 center in the excited spin-triplet state without light for temperatures between 5 and 300 K. Consequently, we have not been able to deduce the value of J from the temperature dependence of the Boltzmann distribution of electrons among the singlet and triplet levels.

2. $^{29}\text{Si}-^{16}\text{O}-^{28}\text{Si}$ Configuration

For the case of the $^{29}\text{Si}-^{16}\text{O}-^{28}\text{Si}$ configuration, the approximate eigenvalues of the spin Hamiltonian in Eq. (1) can be determined by perturbation theory. Unfortunately, the nuclear Zeeman interaction has nonzero matrix elements for the operators I_x and I_z which retard the convergence of the higher-order perturbation terms.

In dealing with the EPR hyperfine spectra of spin- $\frac{1}{2}$ centers, it is usually not necessary to include the nuclear Zeeman interaction if the hyperfine interaction is moderately weak ($|\bar{A}| \lesssim 10^{-2} \text{cm}^{-1}$) since its effect on the corresponding EPR hyperfine spectrum is usually not perceptible. In a spin-1

center, the splitting between the $|S=1, M=0; I, m\rangle$ states arises in zeroth order from the nuclear Zeeman interaction and in second order from the hyperfine and electronic spin-spin interactions. In the case of the Si-S1 center, the order in which the allowed and forbidden ^{29}Si hyperfine lines are observed is reversed, depending on whether the nuclear Zeeman interaction has been erroneously neglected or properly included. Since the order in which the allowed and forbidden ^{29}Si hyperfine lines occur is indicative of the signs of the coupling tensors, one can only be assured of deducing the correct sign combinations for the coupling tensors if the nuclear Zeeman interaction is included in the spin Hamiltonian.

In view of this inadequacy of perturbation theory and the importance of the nuclear Zeeman interaction, the eigenvalues to the spin Hamiltonian in Eq. (1) were calculated using a computer program which diagonalizes Hermitian matrices. Because of the difficulties associated with the problem of fitting 30 independent parameters in the spin Hamiltonian of Eq. (1) to the ^{29}Si hyperfine spectrum, additional constraints were imposed on the general coupling tensors in Table I associated with the $^{29}\text{Si}-^{16}\text{O}-^{28}\text{Si}$ configuration. We assumed that \bar{g}_1 , \bar{g}_2 , and \bar{K} could be accurately represented by the numerical values determined from the fine-structure spectrum. With regard to the hyperfine tensors, the asymmetric part of \bar{A}_{11} or \bar{A}_{21} does not necessarily give any coupling between the singlet and triplet states, but any difference between \bar{A}_{11} and \bar{A}_{21} does. Since our analysis of the fine-structure spectrum indicates that there is very little evidence for coupling between the singlet and triplet states, we constrained \bar{A}_{11} and \bar{A}_{21} to be equal. Finally, we assumed that $\bar{\gamma}_1$ is isotropic and equal to $-\mu_n/I$ where $\mu_n = -0.55477$ for ^{29}Si .

The numerical values for \bar{A}_{11} and \bar{A}_{21} tabulated in Table II were determined by minimizing

$$\sum_i [h\nu_{i,\text{expt}} - h\nu_{i,\text{calc}}(H_{i,\text{expt}}, \theta_i, \bar{g}, \bar{K}, \bar{A}, \bar{\gamma})]^2$$

as a function of \bar{A}_{11} and \bar{A}_{21} (five parameters) by a

direct-search minimization procedure. This analysis was carried out on 48 ^{29}Si hyperfine resonances from the X- and K-band Si-S1 spectra for \vec{H} along the [001], [111], and [110] directions.

IV. STRUCTURE OF Si-S1 CENTER

The interpretation of our EPR measurements is presented in this section and indicates that the Si-S1 center is the neutrally charged, excited spin-triplet state of the one-vacancy-oxygen center.

A. Symmetry of Si-S1 Center

The symmetry of a defect is specified by the point group G_{defect} , which contains all of the operations under which the defect is invariant. Furthermore, the host lattice must also be invariant under at least these same operations. In general, the host lattice will be invariant under the operations of the point group G_{lattice} of which G_{defect} is a subgroup. Each point group G can be expressed as the direct product of $\mathcal{S} \times C_i$ or $\mathcal{S} \times C_1$. The group C_1 contains only the identity operator whereas the group C_i also includes the inversion operator. The order of the point group $\mathcal{S}_{\text{lattice}}$ ($\mathcal{S}_{\text{defect}}$) is n_{lattice} (n_{defect}). The ratio R , where

$$R = n_{\text{lattice}}/n_{\text{defect}}, \quad (3)$$

gives the maximum number of distinct spectral lines for a given allowed magnetic dipole transition. This ratio R is the index of the subgroup $\mathcal{S}_{\text{defect}}$ with respect to the group $\mathcal{S}_{\text{lattice}}$.

In the case of the Si-S1 fine-structure spectrum, the maximum number of distinct spectral lines for a given magnetic dipole transition is six when \vec{H} is tilted out of the (110) plane and away from any high-symmetry directions. Since $n_{\text{lattice}} = 24$, the point groups for which $n_{\text{defect}} = 4$ are D_2 , C_{2v} , D_{2h} , C_4 , S_4 , and C_{4h} . Of these, the operations of D_{2h} , C_4 , and C_{4h} do not leave the host lattice invariant and are excluded from further consideration. The point group D_2 is compatible with a defect for which the principal axes of the \vec{g} and \vec{K} tensors would be the $\langle 100 \rangle$ directions. The point group S_4 is compatible with a defect whose \vec{g} and \vec{K} tensors would be axially symmetric about the [001] direction. Clearly, these restrictions on the \vec{g} and \vec{K} tensors are inconsistent with the minimal constraints which are required to describe the Si-S1 fine-structure spectrum. This leaves only the point group C_{2v} , which is compatible with the minimal constraints on the \vec{g} and \vec{K} tensors required to describe the Si-S1 spectrum. Consequently, the symmetry of the Si-S1 center corresponding to the Si-S1 fine structure is specified by the point group C_{2v} .

B. Hyperfine Interactions

For two paramagnetic electrons interacting with a single nucleus, the hyperfine interaction \mathcal{H}_{HF} is¹⁹

$$\begin{aligned} \mathcal{H}_{\text{HF}} = & \frac{16\pi}{3} \mu_B \frac{\mu_n}{I} \mu_N \sum_{k=1}^2 \delta(\vec{r}_k) \vec{S}_k \cdot \vec{I} - 2 \mu_B \frac{\mu_n}{I} \mu_N \\ & \times \sum_{k=1}^2 \left[\frac{\vec{S}_k \cdot \vec{I}}{r_k^3} - \frac{3(\vec{I} \cdot \vec{r}_k)(\vec{S}_k \cdot \vec{r}_k)}{r_k^5} \right] \\ & + 2 \mu_B \frac{\mu_n}{I} \mu_N \sum_{k=1}^2 \frac{\vec{L}_k \cdot \vec{I}}{r_k^3}. \quad (4) \end{aligned}$$

The first term is the Fermi-contact hyperfine interaction which makes an isotropic contribution to the hyperfine coupling tensors. The second term accounts for the magnetic dipole-dipole interaction between the magnetic moment of the nucleus and the intrinsic magnetic moment of the electron. The \vec{r}_k is the position vector of the k th electron with respect to the nucleus. The second term makes a symmetric contribution to the hyperfine coupling tensors. The third term arises from the magnetic dipole-dipole interaction between the magnetic moment of the nucleus and the orbital magnetic moment of the electron. In conjunction with the spin-orbit interaction, this term can make a second-order asymmetric contribution to the hyperfine coupling tensors.⁹ The asymmetric contribution to the hyperfine coupling tensors of the Si-S1 center is expected to be small because the orbital angular momentum for this defect is nearly quenched as evidenced by the small deviations in the \vec{g} tensors from 2.0023.

In order to match \mathcal{H}_{HF} with the hyperfine interactions in Eq. (1), \mathcal{H}_{HF} is integrated only over the spatial part of $|\Psi(\vec{x}_1, \vec{x}_2) \cdots\rangle$. If the interaction between the singlet and triplet states is weak, which happens to be the case for the Si-S1 center, then the spatial part of $|\Psi(\vec{x}_1, \vec{x}_2) \cdots\rangle$ can be represented to a first approximation by

$$\Psi(\vec{x}_1, \vec{x}_2) = (1/\sqrt{2}) [\chi_1(\vec{x}_1)\chi_2(\vec{x}_2) - \chi_2(\vec{x}_1)\chi_1(\vec{x}_2)]. \quad (5)$$

The one-electron wave functions χ_m can be expressed as a linear combination of atomic orbitals φ_i , where

$$\chi_m = \sum_i \eta_{mi} \varphi_i \quad (6)$$

and l denotes the particular lattice site on which orbital φ_i is centered. The one-electron atomic orbitals for silicon, for example, can be expressed in terms of normalized s , p hybrid orbitals of the form

$$\varphi_i = \alpha_i \psi_{3s,i} + \beta_i \psi_{3p,i}. \quad (7)$$

The isotropic part of the hyperfine interaction a_{kl} between the k th electron and the l th silicon nucleus is a measure of the s -state character in the electronic wave function at the respective nucleus, where

$$a_{ki} = \frac{8}{3} \pi \mu_B (\mu_n/I) \mu_N (\eta_{1i}^2 + \eta_{2i}^2) \alpha_i^2 |\psi_{3s,i}(0)|^2, \quad k=1, 2. \quad (8)$$

The symmetric anisotropic part of the hyperfine interaction $(b_{st})_{ki}$ arises from the non- s -state character in the wave function immediately surrounding the l th silicon nucleus, where

$$(b_{st})_{ki} = \frac{\mu_B \mu_n \mu_N}{I} (\eta_{1i}^2 + \eta_{2i}^2) \beta_i^2 \times \langle \psi_{3p,i} | \frac{3x_s x_t - \delta_{st} r^2}{r^5} | \psi_{3p,i} \rangle, \quad s, t = 1, 2, 3, \quad k = 1, 2. \quad (9)$$

Neglecting the second-order asymmetric contribution, the silicon hyperfine coupling tensors \bar{A}_{ki} are given by the expression

$$(A_{st})_{ki} = \delta_{st} a_{ki} + (b_{st})_{ki}, \quad s, t = 1, 2, 3, \quad k = 1, 2. \quad (10)$$

The asymmetric part of \bar{A}_{11} or \bar{A}_{21} does not necessarily give any coupling between the singlet and triplet states, but any difference between \bar{A}_{11} and \bar{A}_{21} does give nonzero matrix elements of $\bar{S}_1 \cdot \bar{A}_{11} \cdot \bar{I}_1 + \bar{S}_2 \cdot \bar{A}_{11} \cdot \bar{I}_1$ between the singlet and triplet states. Since $\Psi(\vec{x}_1, \vec{x}_2)$ is approximated by the expression in Eq. (5), $|\Psi(\vec{x}_1, \vec{x}_2) \dots\rangle$ is a pure triplet state and implicitly implies that there is no coupling between the singlet and triplet states. Consequently, within the limits of this approximation, \bar{A}_{11} and \bar{A}_{21} are constrained to be equal, as Eq. (10) indicates.

According to Eqs. (8) and (9), the hyperfine interactions give little information about the regions in which χ_1 and χ_2 are small. In the regions of the defect where χ_1 and χ_2 are large enough to give resolved hyperfine spectra, the hyperfine interaction can yield as many as three distinct pieces of information. First, well-resolved hyperfine spectra yield the identity of an isotope by virtue of its nuclear spin and natural abundance. Second, the position of the isotope in the defect can often be deduced from the symmetry of the coupling tensors. And third, the qualitative character of the wave function in terms of its localization and s and p character can be deduced from the hyperfine tensors.

The fact that the Si-S1 center is observed in n - or p -type silicon indicates that neither group-III nor group-V impurities are a constituent in this defect. However, since the intensity of the Si-S1 spectrum was observed to be 20–50 times greater in crucible-grown silicon than the vacuum-float-zone or LOPEX samples that we examined, oxygen is very likely a constituent in the Si-S1 center. Consequently, only the hyperfine spectra due to ^{29}Si and ^{17}O are expected.

1. ^{29}Si Hyperfine Interactions

We have attributed the hyperfine spectrum in Fig. 3 to ^{29}Si . This conclusion is based on the following arguments. The nuclear spin of the isotope responsible for this hyperfine spectrum is $\frac{1}{2}$. The fact that this hyperfine spectrum arises from an isotope of $I = \frac{1}{2}$ on one of two sites is shown unequivocally in Fig. 7 where the ^{29}Si pair hyperfine lines are observed. The intensity of the ^{29}Si hyperfine spectrum relative to the fine-structure spectrum is observed to be 0.097 ± 0.003 . The natural abundance of this isotope as deduced from the intensity of the hyperfine spectrum is $(4.63 \pm 0.15)\%$. The only stable isotope having this spin and natural abundance is ^{29}Si which is 4.70% naturally abundant.²⁰

To a first approximation, the wave function for the two paramagnetic electrons in the Si-S1 center is the product of the antisymmetric wave function $\Psi(x_1, x_2)$ defined in Eq. (5) and the triplet spin states. With respect to the spin-Hamiltonian for-

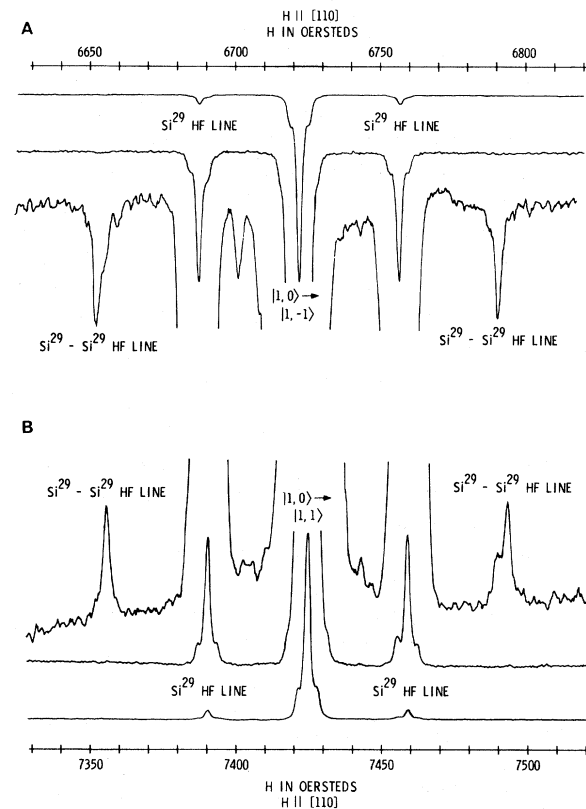


FIG. 7. Part of the Si-S1 spectrum for $\vec{H} \parallel [110]$ showing the fine-structure lines, ^{29}Si hyperfine lines, and the ^{29}Si pair hyperfine lines. This spectrum was observed in $10\text{-}\Omega$ cm P -doped silicon irradiated with $3 \times 10^{17} \text{ e/cm}^2$. The highest-gain traces were obtained using signal-averaging techniques. The A (B) spectrum corresponds to emission (absorption) lines.

TABLE III. Character of wave function in terms of α_i^2 , β_i^2 , η_i^2 as deduced from the ^{29}Si hyperfine interaction.

Spectrum	Sites (Fig. 2)	No. of equivalent sites	a_i (10^{-4} cm^{-1})	b_i (10^{-4} cm^{-1})	α_i^2	β_i^2	$\eta_{1i}^2 + \eta_{2i}^2$
Si-S1	A, B	2	-51.24	-20.79	0.12	0.88	0.64

malism, Eqs. (8)–(10) indicate how $\Psi(\vec{x}_1, \vec{x}_2)$ is contained in the hyperfine tensors \vec{A}_{11} and \vec{A}_{21} . In the case of the Si-S1 center, the \vec{A}_{11} and \vec{A}_{21} tensors are nearly axially symmetric about the [111] direction. If \vec{A}_{11} and \vec{A}_{21} are axially symmetric and equal, then Eq. (9) reduces to

$$b_{\parallel, i} = \frac{4}{5} (\mu_B \mu_n \mu_N / I) (\eta_{1i}^2 + \eta_{2i}^2) \beta_i^2 \langle r_{3p}^{-3} \rangle, \quad (11)$$

and the principal elements of the hyperfine tensors are given by the expressions

$$A_{\parallel, i} = a_i + b_{\parallel, i}, \quad (12)$$

$$A_{\perp, i} = a_i - \frac{1}{2} b_{\parallel, i}. \quad (13)$$

Using the final estimated values of Watkins and Corbett²¹ for $|\psi_{3s}(0)|^2$ and $\langle r_{3p}^{-3} \rangle$ for silicon, some of the values of α_i^2 , β_i^2 , and η_i^2 can be determined from the observed ^{29}Si hyperfine spectra and are tabulated in Table III.

An interpretation of the ^{29}Si hyperfine tensors in terms of the parameters α_i^2 , β_i^2 , and η_i^2 tabulated in Table III gives us an idea of the *s* and *p* character in the *s*, *p* hybrid orbitals ϕ_i and where $\Psi(x_1, x_2)$ is localized. For example, the one-electron orbitals ϕ_1 at *A* and ϕ_2 at *B* are approximately 12% 3*s* and 88% 3*p* in character. Approximately 41% of $|\Psi(x_1, x_2)|^2$ is localized on silicon atoms *A* and *B*. The next-nearest-neighbor ^{29}Si hyperfine spectrum on the sides of the fine-structure resonances in Figs. 1, 4, and 7 is not sufficiently resolved to determine the corresponding ^{29}Si hyperfine tensors. We estimate that the intensity of these hyperfine lines corresponds to six silicon sites. The average magnetic field splitting between these hyperfine lines corresponds to an isotopic hyperfine interaction of $\sim 6 \times 10^{-4} \text{ cm}^{-1}$. We are not certain of the silicon sites to which these ^{29}Si hyperfine lines correspond.

2. ^{17}O Hyperfine Interaction

We have observed the six-line ^{17}O hyperfine spectrum arising from one-vacancy-oxygen centers having the ^{28}Si - ^{17}O - ^{28}Si isotopic configuration (see Fig. 8). The relative abundance of this isotopic configuration was enhanced over that of the ^{28}Si - ^{16}O - ^{28}Si isotopic configuration by incorporating ^{17}O atoms into vacuum-floating-zone silicon by ion implantation. For $\vec{H} \parallel [110]$, the spacing between the ^{17}O hyperfine lines is 14 Oe.

In silicon samples which contain the natural abun-

dance of ^{17}O (0.037%), an ^{17}O hyperfine line in the Si-S1 spectrum would have an intensity of 0.112 with respect to 1.00 for the intensity of a ^{29}Si - ^{29}Si pair line. The resonances in Fig. 7 located 21 Oe above and below the fine-structure resonances agree in both position and intensity with lines in the ^{17}O hyperfine spectrum corresponding to the

$$|S, M; I = \frac{5}{2}, m = \pm \frac{3}{2}\rangle \leftrightarrow |S, M'; I = \frac{5}{2}, m = \pm \frac{3}{2}\rangle$$

transitions. The remaining ^{17}O hyperfine lines are not resolved. These results provide additional¹⁻⁴ evidence for the existence of oxygen in the one-vacancy-oxygen center illustrated in Fig. 2.

C. Electronic Zeeman Interaction

For the case in which the orbital angular momentum of a paramagnetic electron in an orbital single state is quenched, Pryce derived²² the relationship between the actual Zeeman and spin-orbit interactions

$$\mathcal{H}' = \mu_B (\vec{L} + 2\vec{S}) \cdot \vec{H} + \lambda \vec{L} \cdot \vec{S} \quad (14)$$

and the \vec{g} tensor in the electronic Zeeman interaction in the spin Hamiltonian

$$\mathcal{H}_Z = \mu_B \vec{H} \cdot \vec{g} \cdot \vec{S}. \quad (15)$$

The anisotropy in the \vec{g} tensor arises from the admixture of excited states due to the spin-orbit interaction $\lambda \vec{L} \cdot \vec{S}$. To first order in $\lambda \vec{L} \cdot \vec{S}$, the elements in the \vec{g} tensor are given by the expression

$$g_{st} = 2.0023 (\delta_{st} - \lambda \Lambda_{st}), \quad (16)$$

where

$$\Lambda_{st} = \sum_{n \neq 0} \frac{\langle 0 | L_s | n \rangle \langle n | L_t | 0 \rangle}{E_n - E_0}. \quad (17)$$

The adaptation of Watkins's analysis³ of Λ_{st} to the Si-S1 center indicates that the anisotropy in the \vec{g} tensors for the two electrons is given approximately by an expression of the form

$$\Delta \vec{g} \propto \begin{bmatrix} \hat{X}_D \\ \hat{Y}_D \\ \hat{Z}_D \end{bmatrix}^\dagger \begin{bmatrix} 3 & 0 & 0 \\ 0 & 1 & \pm 2 \\ 0 & \pm 2 & 2 \end{bmatrix} \begin{bmatrix} \hat{X}_D \\ \hat{Y}_D \\ \hat{Z}_D \end{bmatrix}. \quad (18)$$

The minus (positive) sign goes with silicon atom *A* (*B*) in Fig. 2.

The results of our analysis on the Si-S1 fine-structure spectrum indicate that $\Delta g_{xx} = 0.0079$, $\Delta g_{yy} = 0.0035$, and $\Delta g_{zz} = 0.0053$ are in the ratios of

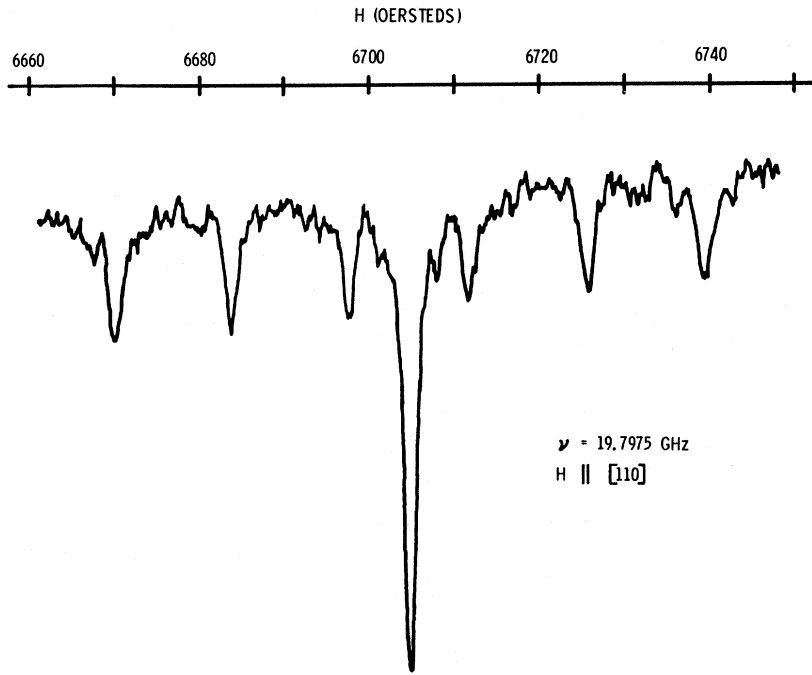


FIG. 8. Si-S1 spectrum for $\vec{H} \parallel [110]$ in the vicinity of 6710 Oe. The central resonance is the fine-structure line corresponding to the $^{28}\text{Si}-^{16}\text{O}-^{28}\text{Si}$ isotopic configuration. The six satellite lines correspond to the ^{17}O hyperfine spectrum and arise from the $^{28}\text{Si}-^{17}\text{O}-^{28}\text{Si}$ isotopic configuration. The enhancement of ^{17}O (natural abundance, 0.037%) over that of ^{16}O (natural abundance, 99.759%) was accomplished using the techniques of ion implantation.

2.84 : 1.26 : 1.91, respectively. These ratios are in good qualitative agreement with the ratios of the corresponding diagonal elements in Eq. (18). The anisotropy and symmetry of the observed \vec{g} tensors are consistent with an odd-vacancy (oxygen) defect for the Si-S1 center. The off-diagonal elements in the \vec{g} tensors associated with the $^{28}\text{Si}-^{16}\text{O}-^{28}\text{Si}$ configuration give only nonzero matrix elements between the singlet and triplet manifolds. As indicated earlier (see Sec. III C), the effect of this interaction on the observed Si-S1 fine-structure spectrum is negligible. Since g_{yz} and g_{xy} are expected to be of the order of ~ 0.004 , and a statistical analysis of our data indicates that g_{yz}^2/J and $g_{xy}^2/J < 10^{-4}$ to 10^{-5} , these relationships suggest that $J > 1 \text{ cm}^{-1}$. This is a rather weak constraint on the lower limit for J .

D. Spin-Spin Interaction

The electronic spin-spin interaction in Eq. (1) can be written in the form

$$\vec{S}_1 \cdot \vec{K} \cdot \vec{S}_2 = J \vec{S}_1 \cdot \vec{S}_2 + \vec{S}_1 \cdot \vec{D} \cdot \vec{S}_2 + \vec{S}_1 \cdot \vec{\alpha} \cdot \vec{S}_2, \quad (19)$$

where $J = \text{Tr} \frac{1}{3}(\vec{K})$, \vec{D} is symmetric with $\text{Tr}(\vec{D}) = 0$, and $\vec{\alpha}$ is antisymmetric. The first term arises from the direct-exchange interaction between the two electrons. The fact that the Si-S1 center is diamagnetic in its ground state indicates that $J > 0$.

A theory of the anisotropic superexchange interaction which takes into account spin-orbit coupling has been developed by Moriya.²³ Moriya has shown²³ that the order of magnitude contributions

to the \vec{D} and $\vec{\alpha}$ tensors arising from the anisotropic superexchange and direct-exchange interactions are

$$D \sim (\Delta g/g)^2 J, \quad \alpha \sim (\Delta g/g) J. \quad (20)$$

Our analysis of the Si-S1 fine-structure spectrum indicates that the antisymmetric part of the spin-spin interaction is zero within experimental error. The relationships in Eq. (20) suggest that the contributions to the \vec{D} tensor arising from the anisotropic superexchange and direct-exchange interactions are also negligible.

The magnitude, anisotropy, and sign of the observed \vec{D} tensor suggest that the spin-spin interaction is dominated by the magnetic dipole-dipole interaction between the unpaired electrons. The magnetic dipole-dipole interaction \mathcal{H}_{dd} between the two paramagnetic electrons is given by the expression

$$\mathcal{H}_{dd} = \frac{\vec{\mu}_1 \cdot \vec{\mu}_2}{r_{12}^3} - \frac{3(\vec{\mu}_1 \cdot \vec{r}_{12})(\vec{\mu}_2 \cdot \vec{r}_{12})}{r_{12}^5}, \quad (21)$$

where $\vec{\mu}_i = -\mu_B \vec{g}_i \cdot \vec{S}_i$. This interaction can make a contribution to the antisymmetric coupling tensor $\vec{\alpha}$, but its magnitude is generally very small.²³ The experimentally observed \vec{K} tensor for the Si-S1 center is consistent with this generality. The symmetric contribution to the \vec{D} tensor due to this interaction is

$$D_{st} = g^2 \mu_B^2 \sum_{l,m} \sigma_{lm} M_{lm}^{st}, \quad (22)$$

$s, t = 1, 2, 3$ (principal axes),

where

$$\sigma_{lm} = \eta_{1l}^2 \eta_{2m}^2 - \eta_{1l} \eta_{2l} \eta_{1m} \eta_{2m} \quad (23)$$

and

$$M_{lm}^{st} = \langle \varphi_l(\vec{x}_1) \varphi_m(\vec{x}_2) | \frac{\delta_{st}}{\gamma_{12}^3} - \frac{3(\hat{n}_s \cdot \vec{r}_{12})(\hat{n}_t \cdot \vec{r}_{12})}{\gamma_{12}^5} | \varphi_l(\vec{x}_1) \varphi_m(\vec{x}_2) \rangle. \quad (24)$$

Equations (22)–(24) do not take into account contributions arising from the overlap of φ_l and φ_m ($l \neq m$).

Since even- and odd-vacancy (oxygen) defects can be distinguished by the symmetry and anisotropy in their g and A tensors, the number of intermediate (oxygen) vacancies in either an odd- or even-vacancy (oxygen) defect can be estimated from the magnetic dipole-dipole interaction. So far, our analysis of the Si-S1 spectrum indicates that the Si-S1 center is an odd-vacancy oxygen center having C_{2v} symmetry. In Table IV, the principal values of the D tensor are tabulated for the one-vacancy-oxygen center illustrated in Fig. 2 and a three-vacancy-oxygen center. With respect to Fig. 2, the end silicon atoms of a three-vacancy-oxygen center would be separated by three intervening vacancies in the $Y_D Z_D$ plane with perhaps an oxygen atom bonded between silicon atoms c and d . With respect to Table IV, the point dipole model for $\Psi(\vec{x}_1, \vec{x}_2)$ assumes that φ_A^2 and φ_B^2 can be represented by Dirac δ functions $\delta(\vec{x}_1 - \vec{x}_A)$ and $\delta(\vec{x}_2 - \vec{x}_B)$, respectively. Since the geometrical extent of the one-vacancy-oxygen center is comparable in size to the extent of the wave function, it is appropriate to calculate the D_{st} by taking into consideration the spatial extent of $\Psi(\vec{x}_1, \vec{x}_2)$. In this case, we represented the one-electron orbitals for the paramagnetic electrons by $3s$, $3p$ hybrid Slater orbitals whose localization and $3s$ and $3p$ character agreed with that deduced from the ^{29}Si hyperfine interactions. The matrix elements in Eq. (24) were numerically evaluated with the aid of a computer. Although only about 41% of $\Psi(\vec{x}_1, \vec{x}_2) \Psi(\vec{x}_1, \vec{x}_2)$ is localized on silicon atoms A and B , the magnitude of the principal values of D_{st} are dominated by that part of $\Psi(\vec{x}_1, \vec{x}_2)$ which is localized on silicon atoms A and B . This is because

the magnetic dipole-dipole interaction goes as $\sim 1/\gamma_{12}^3$. A comparison between the calculated and experimental values for D_{st} in Table II suggests that the one-vacancy-oxygen center is the appropriate model for the Si-S1 center.

E. Stress Dependence

The time-temperature dependence in the reorientation of a defect under stress is a characteristic which is unique to its structure and charge state. The reorientation of the one-vacancy-oxygen center corresponds to a change in the bonding of the oxygen atom between silicon atoms c and d in Fig. 2 to another pair of adjacent silicon atoms (e.g., a and c). Although the Si-B1 spectrum corresponds to the negatively charged one-vacancy-oxygen center, Watkins and Corbett³ have measured the time-temperature dependence in the reorientation of the neutral one-vacancy-oxygen center from the Si-B1 spectrum. Corbett *et al.*⁴ were able to correlate the 12- μ infrared absorption band with the neutral one-vacancy-oxygen center through the time-temperature dependence in the reorientation of this defect.

If the Si-S1 center is the neutral charge state of the Si-B1 center rather than some other defect structure such as a three-vacancy-oxygen center, then the realignment of this center as monitored by the Si-S1 and -B1 spectra should be the same. The experiment described below was performed to test this hypothesis. A sample of n -type crucible-grown silicon was electron irradiated to a fluence for which $\sim 90\%$ of the one-vacancy-oxygen centers formed were in the neutral charge state. In such a sample, the Si-B1 spectrum can be used to monitor the time-temperature dependence in the reorientation of the neutral one-vacancy-oxygen center. Without stress, the relative intensities of the observed resonances in the Si-B1 and -S1 spectra for $\vec{H} \parallel [001]$ were measured. For $\vec{H} \parallel [001]$, there are only two nonequivalent orientations of the one-vacancy-oxygen center. With respect to Fig. 2, the bonding of the oxygen atom between silicon atoms c and d or a and b gives one resonance for $\vec{H} \parallel [001]$ which is associated with one-vacancy-oxygen centers in coordinate frames 1–4. The bond-

TABLE IV. Calculated values for the spin-spin interaction between two electrons assuming a magnetic dipole-dipole interaction. The principal axes are defined with respect to the crystallographic axes in Fig. 2.

Defect	Point dipole approximation D tensor (in units of 10^{-4}cm^{-1})			s, p hybrid orbital approximation D tensor (in units of 10^{-4}cm^{-1})		
	D_{xx}	D_{yy}	D_{zz}	D_{xx}	D_{yy}	D_{zz}
one-vacancy-oxygen	306	-612	306	210	-423	213
three-vacancy-oxygen	38	-76	38	27	-56	29

ing of the oxygen atom between the remaining adjacent pairs of silicon atoms (e.g., a and c , c and b , b and d , d and a) gives the other resonance which is associated with one-vacancy-oxygen centers in coordinate frames 5-12 for $\vec{H} \parallel [001]$. In Fig. 9, the relative intensities of the observed resonances in the Si-B1 and -S1 spectra are plotted corresponding to zero fractional alignment. Zero fractional alignment corresponds to the situation in which the intensity of the resonances corresponds to a random distribution in the orientation of the one-vacancy-oxygen centers. Since the Si-B1 spectrum is observed under conditions of thermal equilibrium, the relative intensities of these resonances are proportional to the number of degenerate coordinate frames. However, the intensity of the corresponding resonances in the Si-S1 spectrum are weighted differently because the excited triplet levels are populated by light (see Sec. III B).

Next, the sample was stressed along the $[1\bar{1}0]$ direction to 880 kg/cm^2 at 135 K for 10^3 sec . At this temperature, the relaxation time for the reorientation of the neutral one-vacancy-oxygen center is $\sim 10^2 \text{ sec}$.³ Within this time and temperature domain no significant reorientation of the

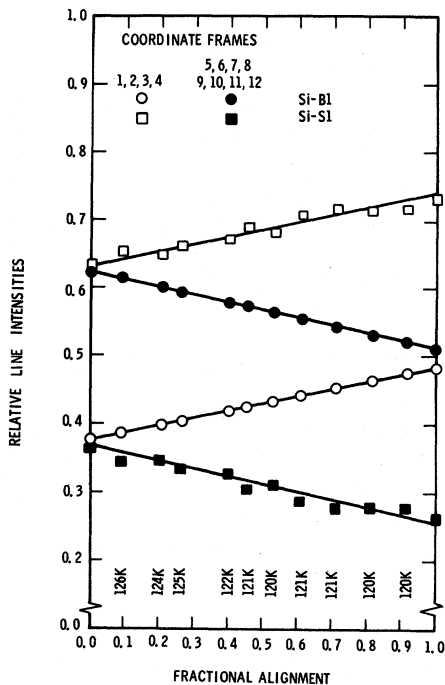


FIG. 9. Plot of the relative intensities of the Si-B1 and -S1 resonances for $\vec{H} \parallel [001]$ vs the fractional alignment of the Si-B1 centers. The fractional alignment of 1 corresponds to the maximum alignment that can be achieved with a stress of 880 kg/cm^2 along with $[1\bar{1}0]$ at $\sim 135 \text{ K}$. The fractional alignment was gradually reduced by annealing the sample at each successive temperature for 30 min.

negative one-vacancy-oxygen center occurs. With stress still applied, the temperature was lowered to $\sim 100 \text{ K}$ and the stress then removed. At 100 K , the characteristic reorientation time of the neutral one-vacancy-oxygen center is $\sim 10^6 \text{ sec}$ while the characteristic electronic redistribution time is $\sim 10^{-5} \text{ sec}$.³ At this temperature, the available electrons hop randomly among all of the one-vacancy-oxygen centers so that on the average these defects are in the neutral charge state $\sim 90\%$ of the time. As the temperature is lowered below $\sim 70 \text{ K}$, the available electrons freeze out randomly among the one-vacancy-oxygen centers. This puts approximately 10% of these defects in the negative charge state. At 25 K where the Si-B1 and -S1 spectra were recorded, the changes in the relative intensities of these resonances reflect the amount of alignment induced by the stress. The relative intensities of the resonances in the Si-B1 and -S1 spectra for $\vec{H} \parallel [001]$ are plotted in Fig. 9 corresponding to a normalized fractional alignment of 1, which is by definition the maximum alignment that can be achieved at this stress and temperature.

The next series of measurements involved measuring the relative intensities of these resonances after the sample was annealed at each of the successive temperatures indicated in Fig. 9 for 30 min beginning with 120 K . The data in Fig. 9 show that the lines representing the recovery in the Si-S1 and -B1 centers in the same sets of coordinate frames (open symbols or closed symbols) are parallel within experimental error. This means that the centers which give rise to the Si-B1 and -S1 spectra have the same time-temperature dependence in their reorientation while in the neutral charge state and implies that these spectra arise from the same basic defect. This result indicates that the Si-S1 center is the neutral charge state of the one-vacancy-oxygen center. If the Si-S1 center were a three-vacancy-oxygen center, the plane containing the vacancy string would also have to reorient. Defects such as the phosphorus vacancy²¹ and divacancy²⁴ which involve more extensive atomic rearrangements are observed to reorient for times of the order of $\geq 1 \text{ sec}$ near room temperature.

V. SUMMARY AND CONCLUSIONS

The Si-S1 spectrum was analyzed in terms of the spin Hamiltonian in Eq. (1). The most general forms of the coupling tensors were derived for the $^{28}\text{Si}-^{16}\text{O}$ - ^{28}Si and $^{29}\text{Si}-^{16}\text{O}$ - ^{28}Si configurations consistent with the C_{2v} and C_s symmetry of these isotopic configurations within the silicon lattice. Although nonzero matrix elements can exist between the triplet and singlet manifolds, the influence of these terms on the Si-S1 spectrum is negligible within the accuracy of our measurements. Con-

sequently, one is justified in describing the Si-S1 spectrum in terms of the reduced coupling tensors tabulated in Table I. The numerical values for the coupling tensors as deduced from the Si-S1 spectrum are tabulated in Table II.

An analysis of the coupling tensors in terms of the actual physical interactions suggests that the Si-S1 center corresponds to the neutral one-vacancy-oxygen center in an excited spin-triplet state. In particular, the lack of any measurable contribution to the antisymmetric part of the \bar{K} tensor indicates, according to Moryia's theory of superexchange, that the superexchange as well as the exchange interactions do not make significant contributions to the \bar{D} and \bar{a} tensors in Eq. (19). The sign, magnitude, and anisotropy of the \bar{D} tensor suggest that the spin-spin interaction is dominated by the magnetic dipole-dipole interaction. We have found that the calculated value for the \bar{D} tensor, assuming a one-vacancy-oxygen model for the Si-S1 center, agrees qualitatively with the observed spin-spin interaction. The phenomenological wave function used in this calculation was deduced from the ^{29}Si hyperfine interactions.

The existence of oxygen in the Si-S1 center has been shown directly from EPR measurements of

the ^{17}O hyperfine spectrum in samples of intrinsic vacuum-float-zone silicon implanted with ^{17}O . In the case of the neutral one-vacancy-oxygen center in an excited spin-triplet state, a resolvable ^{17}O hyperfine interaction exists because one of the one-electron wave functions χ_m transforms as Γ_1 .

The time-temperature dependence in the reorientation of the Si-S1 center under stress confirms that this defect corresponds to the neutral one-vacancy-oxygen center. Our measurements indicate that the time-temperature dependence in the reorientation of the Si-S1 center is the same as that of the neutral one-vacancy-oxygen center as monitored by the Si-B1 spectrum.

ACKNOWLEDGMENTS

The competent assistance of N. D. Wing who carried out the EPR measurements is very much appreciated. Appreciation is also expressed to F. L. Vook, D. K. Brice, and H. J. Stein for helpful suggestions on various aspects of this work. The assistance and advice of W. Beezhold and A. Bromberg with the ^{17}O implants and the use of the ion implantation facilities in Division 5112 are gratefully acknowledged.

[†]Work supported by the United States Atomic Energy Commission.

¹G. Bemski, *J. Appl. Phys.* **30**, 1195 (1959).

²G. D. Watkins, J. W. Corbett, and R. M. Walker, *J. Appl. Phys.* **30**, 1198 (1959).

³G. D. Watkins and J. W. Corbett, *Phys. Rev.* **121**, 1001 (1961).

⁴J. W. Corbett, G. D. Watkins, R. M. Chrenko, and R. S. McDonald, *Phys. Rev.* **121**, 1015 (1961).

⁵G. D. Watkins, in *Radiation Damage in Semiconductors*, edited by P. Baruch (Academic, New York, 1964), p. 97.

⁶N. Almeleh and B. Goldstein, *Phys. Rev.* **149**, 687 (1966).

⁷D. F. Daly and H. E. Noffke, *Bull. Am. Phys. Soc.* **15**, 94 (1970); *Rad. Effects* **8**, 203 (1971).

⁸M. H. L. Pryce, *Nuovo Cimento* **6**, 817 (1957).

⁹F. K. Kneubühl, *Physik Kondensierten Materie* **1**, 410 (1963).

¹⁰F. K. Kneubühl, *Physik Kondensierten Materie* **4**, 50 (1965).

¹¹A. Bieri and F. K. Kneubühl, *Physik Kondensierten Materie* **4**, 230 (1965).

¹²H. P. Baltes, J. F. Moser, and F. K. Kneubühl, *J. Phys. Chem. Solids* **28**, 2635 (1967).

¹³The resonances in the Si-S1 spectrum which are observed at the same audio phase in the same samples with the same polarity as the resonances in the Si-B1, -G7, -G15, and -G18 spectra are defined as absorptive

resonances.

¹⁴D. H. Tanimoto, W. M. Ziniker, and J. O. Kemp, *Phys. Rev. Letters* **14**, 645 (1965).

¹⁵G. D. Watkins, *Phys. Rev.* **155**, 802 (1967).

¹⁶For a defect in silicon whose symmetry is specified by the lowest symmetry point group C_1 , the maximum number of distinct spectral lines for a given allowed magnetic dipole transition is 24 (see Sec. IV A). If the EPR spectrum is recorded with H in a (110) plane, then the maximum number of distinct spectral lines for a given allowed magnetic dipole transition is 12. Other degeneracies may exist, depending on the symmetry of the defect and the direction of the magnetic field.

¹⁷Varian Associates, *NMR Table*, 4th ed., 1964 (unpublished).

¹⁸H. Margenau and G. M. Murphy, *The Mathematics of Physics and Chemistry* (Van Nostrand, Princeton, N. J., 1956), p. 517.

¹⁹B. Bleaney and K. W. H. Stevens, *Rept. Progr. Phys.* **18**, 108 (1953).

²⁰R. B. Leighton, *Principles of Modern Physics* (McGraw-Hill, New York, 1959), p. 736.

²¹G. D. Watkins and J. W. Corbett, *Phys. Rev.* **134**, A1359 (1964).

²²M. H. L. Pryce, *Proc. Phys. Soc. (London)* **A63**, 25 (1950).

²³T. Moriya, *Phys. Rev.* **120**, 91 (1960).

²⁴G. D. Watkins and J. W. Corbett, *Phys. Rev.* **138**, A543 (1965).